A FAST RIGHT VENTRICLE SEGMENTATION IN CINE-MRI FROM A DENSE HOUGH REPRESENTATION

Jean Alejandro Pico-Velásquez*[1], Alejandra Moreno-Tarazona*[2], Luis Carlos Guayacán-Chaparro*[3], Lola Xiomara Bautist-Rozo*[4], Fabio Martínez-Carrillo*[5]

[1]Ingeniero de Sistemas. Estudiante UIS. Bucaramanga, Colombia. jean.pico@saber.uis.edu.co
[2]Ingeniera de Sistemas. Estudiante UIS. Bucaramanga, Colombia. alejandra.moreno@saber.uis.edu.co
[3]Magister en Matemática Aplicada. Estudiante UIS. Bucaramanga, Colombia. luis.guayacan@saber.uis.edu.co
[4]Doctora en Ciencias. Docente UIS. Bucaramanga, Colombia. lxbautis@uis.edu.co
[5]Doctor en Sistemas y Computación. Docente UIS. Bucaramanga, Colombia. famarcar@uis.edu.co
*Grupo de Investigación BIVL[2]ab, Universidad Industrial de Santander (UIS)

ABSTRACT

Right ventricle (RV) segmentation is essential for the diagnosis of multiple cardiac pathologies and conditions. However, RV manual delineation is a tedious task and the design of computational support tools is challenging due to geometric and dynamic variability. This work introduces a representation based on the dense Hough transform (DHT) that allows a non-parametric characterization of the shape, encoding each voxel by its curvature and orientation. This representation is integrated into a Bayesian tracking approach, which efficiently segments the RV structure throughout the cardiac cycle. The proposed approach was evaluated on a public dataset, with 16 patients, achieving a Sørensen-Dice coefficient of 0.87 and 0.92, for complete volumes and basal structures, respectively. These results evidence an adequate fit of the proposed model with respect to RV shape throughout the entire cardiac cycle.

UNA SEGMENTACIÓN RÁPIDA DEL VENTRÍCULO DERECHO EN CINE-MRI A PARTIR DE UNA REPRESENTACIÓN DENSA DE HOUGH

RESUMEN

La segmentación del Ventrículo Derecho (VD) es esencial para el diagnóstico de múltiples patologías y condiciones cardiacas. Sin embargo, su delineación manual es una tarea tediosa y el soporte computacional resulta complejo debido a la variabilidad geométrica y dinámica. Este trabajo introduce una transformación y representación densa de Hough (TH) que permite una caracterización no paramétrica de la forma, codificando cada vóxel por su curvatura y orientación. Esta representación es integrada en un enfoque de seguimiento bayesiano, que logra de forma eficiente segmentar la estructura del VD, a lo largo del ciclo cardíaco. El enfoque propuesto fue evaluado en un conjunto de datos públicos, con 16 pacientes, logrando un coeficiente Sørensen-Dice de 0,87 y 0,92, para volúmenes completos y estructuras basales, respectivamente. Estos resultados evidencian una adecuada adaptación del modelo propuesto respecto a la forma del VD a lo largo de todo el ciclo cardíaco.

Como citar este artículo: Pico-Velásquez, J., A., Moreno-Tarazona, A., Guayacán-Chaparro, L., C., Bautist-Rozo, L., X., & Martínez-Carrillo, F. (2022). A fast right ventricle segmentation in cine-mri from a dense hough representation, 18(35), 84-97. https://doi.org/10.33571/rpolitec.v18n35a6

1. INTRODUCTION

Cardiovascular diseases (CVDs) are the main cause of death around the world, according to the World Health Organization (WHO). About 17.9 million people die each year from CVDs, corresponding to 31% of all deaths worldwide [1]. The analysis of the structural and dynamic patterns of the heart is crucial to evaluate its functionality, supporting the diagnosis and prognosis of associated diseases. Currently, characterization of the right ventricle (RV) has proven to be one of the main ways to analyze these spatio-temporal patterns and support diagnostic decisions [2,3,4]. For instance, volumetric RV patterns support the characterization of pulmonary hypertension, cardiomyopathy, myocardial infarction, and congenital heart diseases [5,6,7]. However, the first step to assess RV is the contour delineation task, which is a tedious expert-dependent task that introduce inter and intra-observer variability [8]. Additionally, during the clinical routine, the RV delineation could take more than 15 minutes for each patient [4].

Hence, computational tools are required to automatically delineate RV structures and efficiently support clinical procedures [9]. This is a challenging task because of the high dynamic and structural variability of RV. Additionally, the low resolution of cine-MRI acquisitions difficult to track non-linear cardiac dynamics. Moreover, trabecular muscles, are not well separated from the RV wall [10]. In fact, in almost all studies, RV delineation is only performed during end-diastole and end-systole, that is, when the greatest relaxation or contraction of the ventricular cavities occurs, losing information about global structural changes during time.

In the literature, global segmentation strategies have been mainly applied to delineate the RV, exploring from different statistical shape models that involve likelihood appearance measures [8,11]. In these approaches, a set of manual delineations built a statistical model that is matched over a new cine-MRI according to some predefined rules on image space. These approaches achieved a proper global matching but lacked local shape definition due to the high RV variability across different spatial and temporal slices, as well as the variability among patients. Additionally, atlas-based strategies index a set of training samples with associated delineations that are individually mapped to the new cine-MRI, using registration techniques. In such a case, the delineation of an atlas image with minimal transformation w.r.t the new volume is set as a new segmentation. These approaches overcome noise and low tissue-to-blood contrast problems but namely report several limitations regarding the adaptation of local template details [12,13].

These alternatives use prior anatomical information to guide the segmentation process. For instance, Petit Jean et al. [4] proposed an automatic segmentation method based on multi-label graph cuts, which makes use of a probabilistic shape model. First, atlas examples are non-rigid registered with respect to unknown images. Then, a probabilistic model based on the registered images is created and a shape model is obtained by merging several atlases after their non-rigid registration on the unknown image. Finally, this prior is incorporated into the multi-label graph cut framework in order to guide the segmentation. The main advantage of this method is the low computational cost. Nevertheless, the performance and results of this methodology mainly depends on the method used for the non-rigid registration.

Likewise, machine learning approaches have been proposed to carry out RV segmentation. Particularly, convolutional neural networks (CNNs) have achieved record-breaking accuracy performances. For instance, Zhen et al. [14] proposed a directed bi-ventricular volume prediction method based on CNNs and random forests. Their method takes advantage of both, unsupervised representation learning and supervised volume estimation. Avendi et al. [15] proposed a method based on CNN and a stacked autoencoder, which is trained to locate the region of interest (RoI) and delineate efficiently the boundary of RV. Although these methods obtain remarkable results and they have the ability to perform transfer learning, CNNs based approaches require a considerable amount of data for training and are highly dependent on the implemented architecture.

The main contribution of this work is a robust and fast Hough representation that follows, captures and delineates the complex RV shape along the cardiac cycle. The method starts by matching an average template over the initial frame of the cine-MRI. Such template allows us to coarsely localize and define the structure of the RV and the surrounding regions, i.e., the background. Hence, a dense Hough transform (DHT) codes ventricle information from local curvature and orientation into the region of interest. These primitives are accumulated in representation tables (R-Tables) to follow the structure along time and considering non-parametric shapes. From that region of interest, a spatial and motion deformation model is described as a recursive Bayesian strategy. The DHT is also back-projected to define a coarse RV segmentation that complements and updates the appearance observation model.

2. MATERIALS AND METHODS

The structure and function of the right ventricle play an essential role in the diagnosis and monitoring of many cardiovascular diseases. However, the complex RV dynamic and its non-parametric shape make difficult the segmentation process. In this work is introduced a low-level heart representation using a temporal Bayesian framework through a multi-scale DHT. This transformation is operated pixel-wise into a multi-scale scheme that allows following non-parametric shapes along time. From such local representation, it is possible to characterize cardiac structures that exhibit complex spatial and temporal patterns. Then a probabilistic model is implemented to segment RV from the background. At each time, the DHT and probabilistic model are complemented and updated to achieve a temporal segmentation. The following subsection describes in detail the steps of the proposed RV segmentation.

2.1. RoI estimation: rigid training initialization: First, a set of new cine-MRI training sequences is rigidly registered as an atlas-based approach. Then, the initial localized RoI (Ω), is herein used to learn an RV template ζ_x to avoid undesired deformations of its morphology, following a dense per-voxel Hough representation. This template ζ_x is modeled over each RV heart contour given by a physician expert. Finally, the non-rectangular RoI (Ω) is estimated according to a transformed contours average of samples, *i.e.,* $X_{avg} = \frac{1}{N}\Sigma_{i=1}^{N}X_i$ where i corresponds to each sample of a training sequence. In Figure 1 is illustrated the process of rigid registration of a set of training samples w.r.t a target. The initial delineation, taken from the average, is then characterized with the DHT and evolved according to a statistical framework.
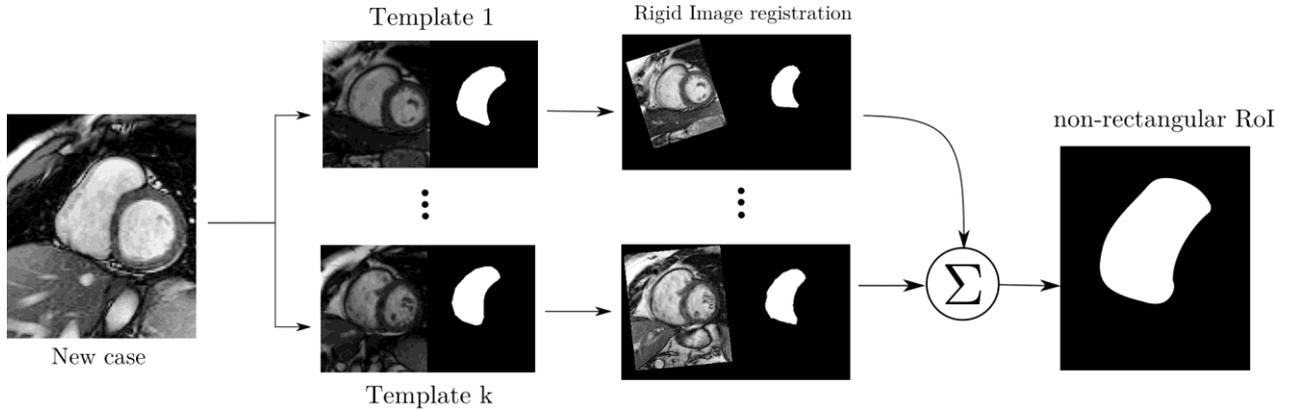

Figure 1: Automatic non-rectangular RoI estimation. First, the dataset volumes are rigidly registered w.r.t the target (New case). Then, all contours are transformed to fit the target. Finally, an average between all contours is computed to obtain a non-rectangular RoI estimation Ω for the new case.

2.2. Dense Hough Transform for heart characterization: In this work is implemented a DHT to capture local heart information by coding curvature and orientation at voxel level. Such characterization is carried out in both: space and time allowing a non-parametric characterization of cardiac structures. Also, this work involves multi-scale evaluation of cardiovascular magnetic resonance (CMR) imaging sequences, as well as analysis of motion primitives and deformations that can be coded in cumulative tables to achieve a robust representation. The heart structures were coded from DHT and used in right ventricle segmentation (see Figure 2).

Firstly, a cine-MRI captures the heart structures together with surrounding organs along the cardiac cycle. A fundamental task is to obtain a representation of the cardiac structures over time, allowing to identify and localize these regions automatically from others in the cine-MRI. An initial delineation of cardiac structures made by an expert cardiac radiologist is taken at the first slice. Then a Dense Hough representation allows to detect and follow the marked regions of interest (RoIs). For doing so, a template ζ_x is computed over a rectangle surrounding RoIs, centered at position x. Since an MRI sequence is a temporal volume, such a template can be computed at every slice where cardiac structure exists or can be computed at independent relevant slices for the analysis (e.g., the basal, mid and apical slices). The characterized template is then used to search and detect the respective RoIs in the whole slice for all cine-MRI volumes.
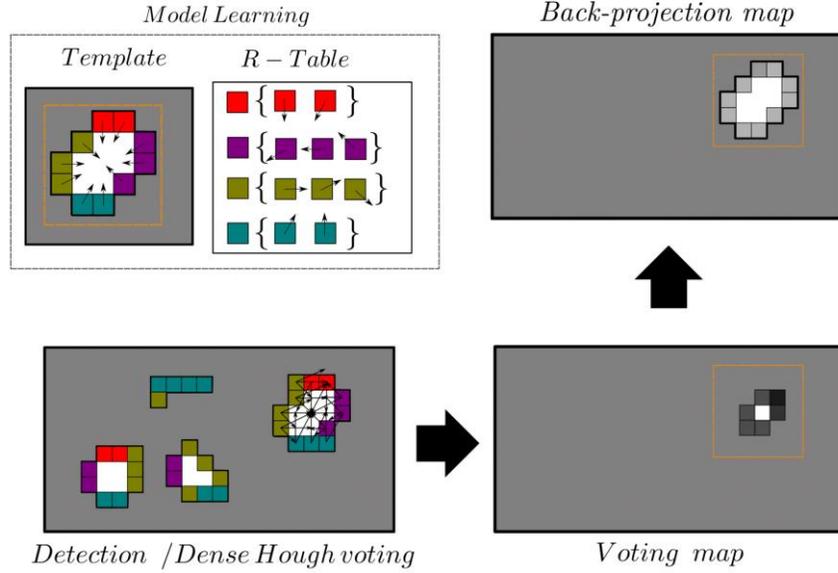
Figure 2: Automatic RV segmentation using DHT. The DHT allows to detect and follow a region that bound the right ventricle. Firstly, some features of a template are calculated at the pixel level and stored together with the distance from each pixel to the center of the template. Then, the same process is performed on each frame extracting the same features. Then, a search in the R-table is performed to obtain the position in which each vote is going to take place. Finally, a back-projection process is performed to recover the pixels that contributed the most in the estimation of the center.

2.2.1 Learning - ζ_x representation: Let be x a pixel location with coordinates (x, y). The template is characterized using a multi-scale framework $\left\{ \zeta_{x,i}^{\sigma} = \zeta_x * \left(\frac{\partial G_g}{\partial x^i} \right) \right\}$ that essentially exploits the spatial structure and features provided by the first and second derivatives at different scales $\sigma = \sigma_1, \ldots, \sigma_n$. This multi-scale approach probed to reduce the influence of spurious structures (e.g., the left ventricle), improving detection [16]. From such template $\zeta_{x,i}^{\sigma}$ is possible to compute local primitives at each location x such as the curvature κ_x and gradient orientation $\theta(\nabla \zeta_{x,i})$ [16].

$$\kappa_x = \frac{\zeta_{xx}\zeta_y^2 - 2\zeta_{xy}\zeta_y\zeta_x + \zeta_{yy}\zeta_x^2}{\|\nabla\zeta_x\|^3} \qquad \textbf{(1)}$$

$$\theta(\nabla\zeta_x) = \begin{cases} \pi + \tan\left(\frac{\zeta_y}{\zeta_x}\right)^{-1}, & if\ \zeta_x\zeta_x < 0. \\ \tan\left(\frac{\zeta_y}{\zeta_x}\right)^{-1}, & otherwise. \end{cases} \qquad \textbf{(2)}$$

From such multi-scale representation, it is possible to perform a more robust search in the next frames to detect the cardiac structures of interest. To do so, two representation tables (RT_n) were defined as accumulators' arrays that count occurrences of gradient orientation (θ_x) and curvature (κ_x) for each pixel, respectively. To limit the size, these features are quantified, and the curvature is bounded to [-1,1]. For R-Tables calculation, those sets of pixels with a gradient magnitude equal to zero are not considered, avoiding non defined value estimations. The algorithm 1 shows systematic construction of the two R-tables. In such case $RT_1\big(\theta(\nabla\zeta_{x,i}), \sigma\big)$ concatenates weighted gradient orientations and relative positions (Δ_x) w.r.t the center. $RT_2(\kappa, \sigma) += \big(\Delta_x, \|H_{Ix}\|\big)$ concatenates information with respect to the curvature index by the Frobenius norm of the Hessian matrix.

Figure 3 illustrates the characterization process for a cardiac structure of interest, e.g., the RV. In this case, all pixels inside the rectangular RoI constitute the template for learning. This process is done once for each MRI volume. These RTs are updated by adding the RV structural changes over time.
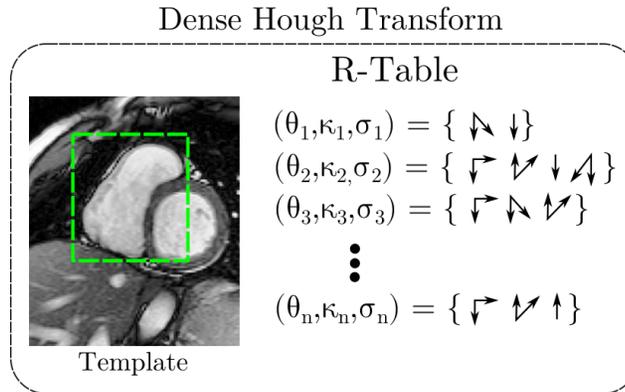

Figure 3: Basal slice: RV characterization example using a rectangular RoI Ω_{dht} as an input of DHT, these *RTs* are updated by adding the RV structural changes over time depending on θ, κ and σ.

2.2.2. Detection - searching ζ_x: From such local RoI characterization it is possible to detect arbitrary non-analytical tissues such as the heart ventricles. Each RT is then projected into each new slice to search for similar features and build an accumulation map (Γ). Every pixel vote, according to its orientation and curvature indexes and its votes, are weighted as indicated in the RT. The local maximum in Γ is then considered as the center of the detected RoI. Algorithm 2 summarizes the automatic detection of RoIs for every slice at each cine-MRI of the dataset.

Figure 4 shows the accumulation map computed for each frame and each slice of the Cine-MRI sequence. Where the brightest pixel at position x represents the RV center with some margin of error.
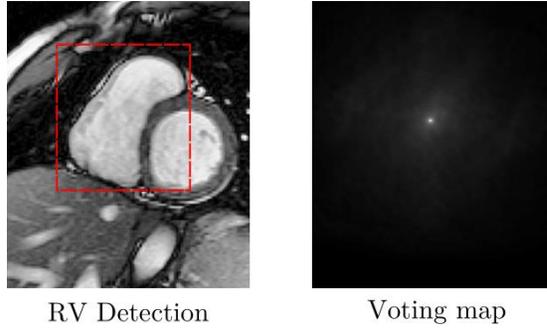
RV Detection   Voting map

Figure 4: Left: RV RoI detected for a Basal slice. Right: Accumulation map which represents the voting process for detection.

2.2.3. Back-projection: From the voting map, it is possible to recover the center of the estimated RoI $\hat{\zeta}_x$ along the cardiac MRI sequence. Then, at each time it is possible to obtain an automatic identification of the selected structure. The pixels that better represent cardiac structures have significant contributions to the voting map. From such an assumption, a non-parametric shape can be recovered from the voting map by selecting the pixels according to each contribution [17]. In the segmentation scenario, a back-projection strategy is implemented from a thresholded version of contributing pixels. This coarse model is used to update the segmentation model that leads to better discrimination of foreground and background pixels into the region of interest.

2.3. Bayesian Segmentation Model: Once the Hough representation is recovered, the main scenario for evaluation is heart chambers segmentation. For doing so, a probabilistic approach is herein implemented with the Hough transformation. The heart shape estimation S_t is involved in a well-defined cardiac cycle description $S_t \rightarrow S_{t-1} \rightarrow S_{t-2}...$, where consecutive shape changes depend on temporal motion and deformation history. Additionally, to history information, at each time t, it is possible to recover a particular observation of the heart $\widehat{S}_{t-1} = S_{t-1} + e$, where e represent noise in the captured measurements. From such analysis, we can approximate the heart dynamic segmentation as a Bayesian inference of first order, described by Chapman-Kolmogórov equation:

$$p_{ij}^n = \sum_{k=0}^{M} p_{ik}^m p_{kj}^{n-m} \quad (3)$$

Where p_{ij}^n represents the transition probability from state i to state j in n steps or iterations. For our case, we assume that heart chambers do not change their shape between frames abruptly. In this assumption, we consider a Markovian first approximation, *i.e.*, the most important information of motion history is in the previous frame $(t-1)$. Like in [17], a segmentation model is adopted which is trained and updated during the cardiac cycle to improve discrimination. For this segmentation model, a recursive Bayesian formulation approach is used, based on tissue-to-blood contrast present in the RoI in a time t. The Bayesian inference allows to increase model robustness by incorporating the information present in previous sequences $(t-1)$. To create this model, two probabilities are defined for each position x, that is, probability of the pixel x to belong to RV (Foreground) and probability of the pixel x to be any other tissue (Background). Let $C_{t,x}$ be the pixel class at the position x at a time t, where $C_{t,x} = 0$ for surrounding tissues and $C_{t,x} = 1$ for RV. Furthermore, be $y_{1_{t,x}}$ the tissue-to-blood contrast information in the position x. The probability of the pixel x pertaining to the right ventricle $\left(P(C_t = 1 \mid y_{1:t})\right)$ is defined by:

$$P_{total} = P(C_t = 1)P(C_t = 1 \mid C_{t-1} = 1) + 1 - P(C_t = 1)P(C_t = 0 \mid C_{t-1})$$

$$(4)$$

$$P(C_t = 1 \mid y_{1:t}) = P_{total} * P(C_{t-1} = 1 \mid y_{1:t})P(C_t = 1 \mid C_{t-1})$$

Let Ω be the RoI obtained in Figure 1. From Ω, two scaled versions are created (Ω_{fg},Ω_{bg}). For the first case $\left(\Omega_{fg} = 1.3 * \Omega\right)$ the inner region is taken, which contains the pixels corresponding to the RV. In the second case, the region resulting from the difference between $1.5 * \Omega$ and Ω_{fg}, i.e., $\Omega_{bg} = 1.5 * \Omega \; xor \; \Omega_{fg}$ is taken. Once Ω_{fg},Ω_{bg} are obtained, color histograms are calculated into these regions, which are normalized and quantified to 12 and 24 bins per region. These histograms contain the tissue-to-blood contrast information necessary for the construction of the model based on Bayesian inference. A prior $P(C_t = 1)$ is initialized in Ω_{fg}. The resulting $P(C_t = 1 \mid y_{1:t})$ can be seen in Figure 5-(a)(c). Thus, the final segmentation is obtained by thresholding this RV probability image (see Figure 5-(b)(d)).
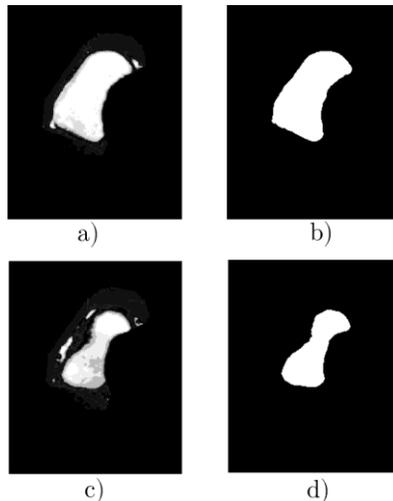

Figure 5: Segmentation model. a) Diastole RV probability; b) Diastole segmentation; c) Systole RV probability; d) Systole segmentation.

The segmentation and Dense Hough (DH) detection models are updated in a complementary manner, i.e., the upgrading of one model depends on the other. The DH model update recalculates the Δ_x displacements within the rectangular RoI Ω_{dht} (Figure 3). In such a case, the weights are then updated using the constraints shown in the equations below. Where if the Δ_x displacements exist in the RT_n model their weight will be updated, otherwise, this displacement will be added to the corresponding RT_n.

$$\omega_1 = \begin{cases} \gamma P(C_x = 1|y)\omega_1 + (1-\gamma)\omega_1, & if \; \Delta_x \in RT_1(\theta,\sigma). \\ \gamma P(C_x = 1|y)\|\nabla I\|, & otherwise. \end{cases}$$

$$\omega_2 = \begin{cases} \gamma P(C_x = 1|y)\omega_2 + (1-\gamma)\omega_2, & if \; \Delta_x \in RT_2(\theta,\sigma). \\ \gamma P(C_x = 1|y)\|HI\|, & otherwise. \end{cases} \tag{5}$$

As RV has several deformations during the MRI sequence, the Hough descriptor should take into account these changes. In Figure 6-(c)(d) is shown how the detection works for a critical scene where the RV has the maximum contraction (end-systole). It is noticeable how the voting map becomes noisier but still detects the RV correctly. In this case, the model was trained for the diastole scenario.

The segmentation model updating uses back-projection map information to update the histograms for RV and non-RV tissues. To do so, only pixels with vital importance or significant influence in the voting map are taken into account; in our case, only greater than 0.5 (in a range from 0 to 1). These pixels increase their importance in the probability model, while the others decrease (as shown in the equation below), turning into a better discrimination. Empirically an update factor $\delta = 0.1$ was chosen.

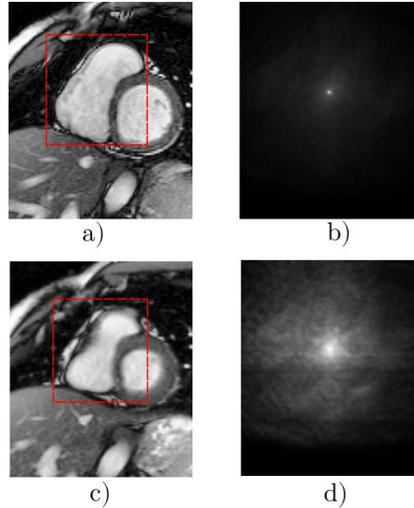$$P(y_t = C_t \mid 1) = \delta P(y \mid b > 0.5) + (1-\delta)P(y_{t-1} \mid C_{t-1} = 1) \tag{6}$$

Figure 6: Hough model updating. a) Diastole cine-MRI; b) Diastole voting map; c) Systole cine-MRI; d) Systole voting map.

2.4 Experimental results: The evaluation of the proposed method was performed over the Right Ventricle Segmentation Challenge (RVSC) dataset which was organized by MICCAI'12 [4]. This consists of a total of 16 patient short-axis volumes and a set of ground truth contours. All patient data were anonymized according to the MICCAI'09 LV segmentation challenge criteria. The CMR study was performed at 1.5T Symphony Tim, Siemens Medical Systems. A conventional 2-chamber view was acquired with a total of 10-14 short-axis slices from Apex to Basal. The examination parameters were the following: TR = 50 ms; TE = 1.7ms; flip angle = 55˚; slice thickness = 7 mm; matrix size = 256 × 216; Field of view (FOV) = 360 mm × 420 mm; 20 images per cardiac cycle. Manual delineation was carried out by an expert cardiologist who manually delineated endocardial and epicardial contours of the RV.

As suggested by dataset authors, two different metrics were herein used to evaluate the performance of the proposed approach: The global Sørensen-Dice coefficient (DSC) and the local Hausdorff Distance (HD). On the one hand, the similarity DSC computes the spatial overlap between two discretely labeled objects. It is a traditional metric for segmentation performance evaluation, where the similarity between the ground truth (GT) and the RV segmentation is measure in a range from 0 to 1 (higher is better), described as $DSC = \frac{2(GT \cap RV_{seg})}{GT + RV_{seg}}$. On the other hand, the HD measures how far two contours are from each other. This metric gives us complementary information of similarity between A and B. Defined as: $HD(A, B) = \max_{a \in A} \left\{ \min_{b \in B} \{ d(a, b) \} \right\}$.

3. EVALUATION AND RESULTS

Firstly, a qualitative evaluation of obtained RV segmentation is illustrated in Figure 7 and Figure 8. In such cardiac cine-MR short-axis images can be observed the performance of the proposed strategy in basal heart regions, being close to expert manual delineations. Also, for different shapes, the strategy is well adapted during the cardiac cycle (Figure 7). The approach can follow and tracking the RV motion and deformation. For apical images, the segmentation represents a greater challenge because of the small regions where the RV RoI is present (Figure 8 - second row). Even for an expert physician, these slices are a tough task. Nevertheless, the proposed approach achieves an appropriate segmentation in these apical regions with some local limitations.
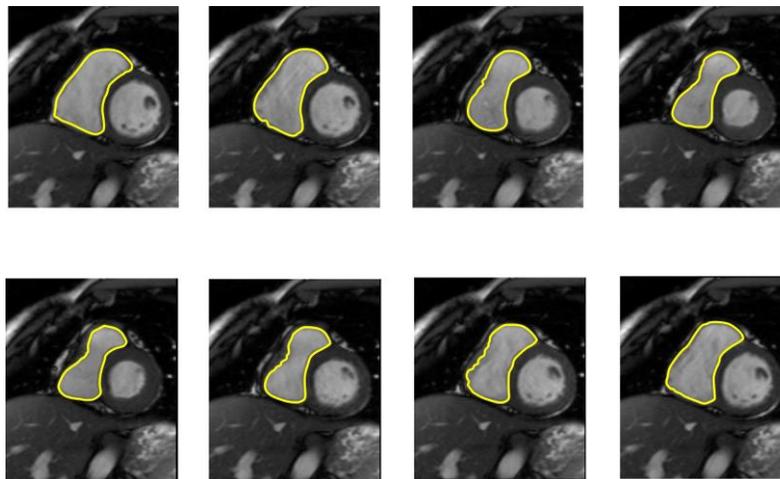
Figure 7: Segmentation results for patient #4 during cardiac cycle. Yellow: proposed RV segmentation.
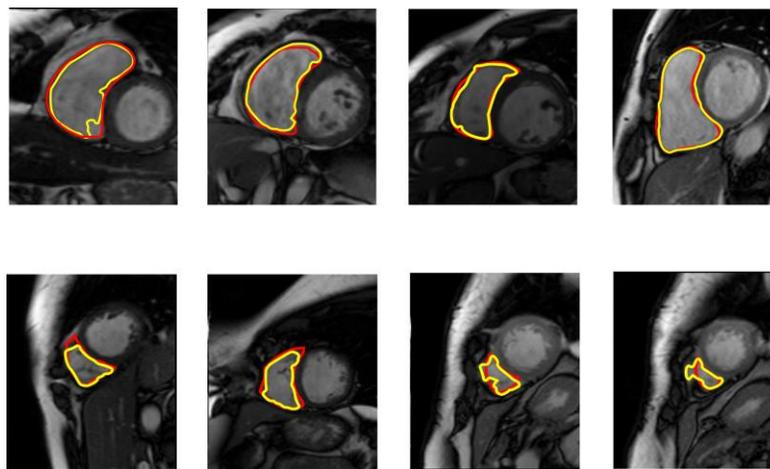
Figure 8: Segmentation results from Basal to Apex. Yellow: proposed RV segmentation; Red: ground truth contour.

Secondly, an exploration was carried out to adjust the proposed approach w.r.t to parameters that are sensitive to the segmentation. The selected parameters evaluated in a spectrum of values are: non-rectangular RoI threshold, non-rectangular RoI scaling factor, color histogram bins, and segmentation threshold, described as follows.

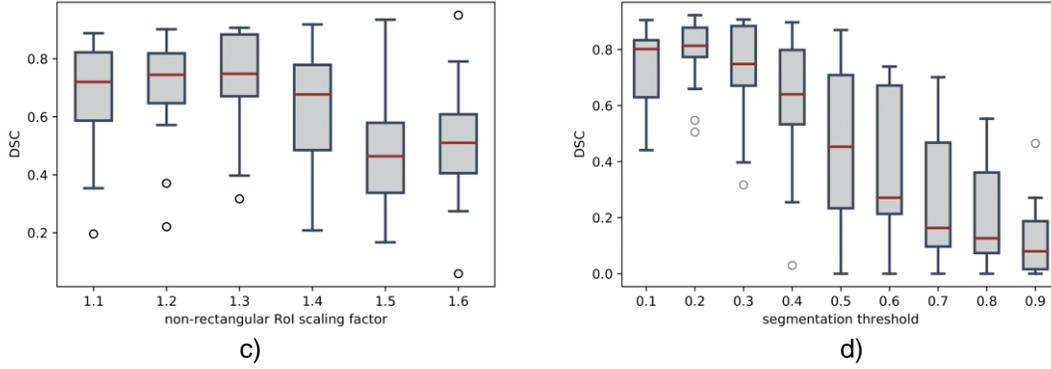c)   d)
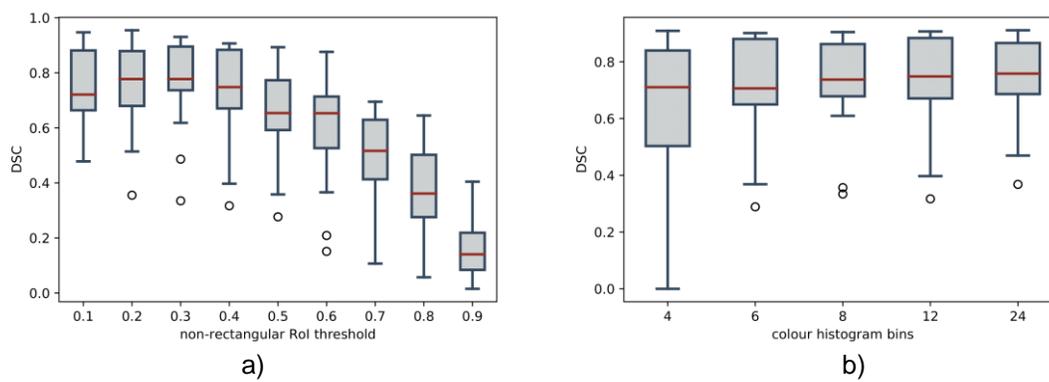
Figure 9: Methodology parameters influence in DSC performance. a) Non-rectangular RoI threshold parameter. b) Color histogram bins parameter. c) Non-rectangular RoI scaling factor parameter. d) Segmentation threshold parameter. Parameters (b), (c) and (d) correspond to the segmentation model.

- **Non-rectangular RoI threshold:** This procedure is applied to the average image contour obtained from the rigid registration. The threshold values are fixed in an interval [0-1]. For values close to zero, a significant area of common delineations is taken into account, while for values close to one, only common values in whole delineations are considered. In Figure 9-a), a value of 0.3 yields the best performance and less data variability, with an average accuracy of 0.81. In such a case, the proposed approach is better when it is possible to admit a larger region to initialize the algorithm.

- **Non-rectangular RoI scaling factor (FG/BG):** to define the size of foreground (FG) and background (BG) area sizes, a RoI scaling factor is computed following the relation $\frac{fg}{bg}$ (see Figure 10). As illustrated in Figure 9-(c), the best result is obtained when the foreground RoI scale is 1.2 times bigger than the background. Statistically, such fact has sense since both regions are well balanced regarding samples to compute the histograms of each region.
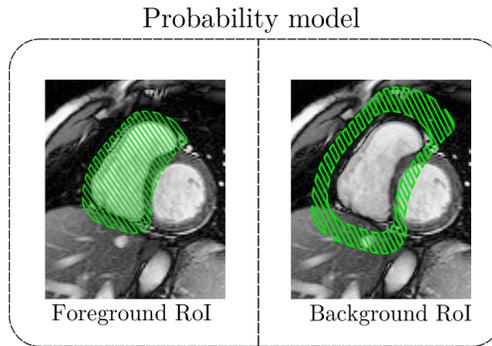

Figure 10: Left: Area Ω_{fg} where the RV histogram is calculated; Right: Area Ω_{bg} where the surrounding tissue histogram is calculated.

- **Color histogram bins:** For the quantization process, necessary to build the tissue-to-blood contrast probability model. Specifically, Ω_{fg} and Ω_{bg} represent histograms quantization. In Figure 9-(b) is shown that the performance remains almost constant for a different number of bins.

- **Segmentation threshold:** This is the final step for segmentation, which selects a set of pixels likely belonging to RV according to its probability of being RV. All pixels below the segmentation threshold are considered surrounding tissue. As expected, lower thresholds allow to take major information of the RV area, leading to better performance of the proposed approach. Being the best performance value $\tau = 0.2$, as shown in Figure 9-(d).

In a third evaluation, the proposed approach was tested with three different configurations by coding different input delineations. The result of these three different configurations is shown in Table 1. In the first case only

one rectangular region was passed without any prior information of the heart shape (Fully rectangular). Interestingly, the proposed approach achieves in average an 88% of accuracy for basal slices, discovering the true shape of the ventricle automatically by only using appearance information.

A second approximation takes into account the information from an initial delineation by computing the DHT overall region. As expected, the result is considerably better with an accuracy of 90% due to the initial consideration of shape. Finally, the best result is achieved when the segmentation model is also updated w.r.t to the information of DHT at each time, i.e., during the cardiac cycle, achieving an accuracy of 92% in average of basal slices and 87% in all cardiac slices. Therefore, the model combines rectangular regions for detection and non-parametric regions for segmentation and updating. It is worth noting the improvement in apical slices by introducing properly prior knowledge of the training delineations.

Table 1. Quantitative comparison results for different RoIs approaches. Rectangular + Non-Rectangular V1 represents a computation of the DHT overall region, meanwhile Rectangular + Non-Rectangular V2 represents the information obtained with the DHT during the cardiac cycle.

RoI Approach	Basal	All slices
Full Rectangular	0.88	0.66
Rectangular + Non-Rectangular V1	0.90	0.76
Rectangular + Non-Rectangular V2	**0.92**	**0.87**

In Table 2 is summarized the Dice Similarity Coefficient (DSC) and Hausdorff Distance (HD) obtained by the proposed approach. A leave-one-out cross-validation was performed. For this, a total of 16 patients with contours from the RVSC dataset were used. The results were split for basal and all slices (basal, mid, and apex). The best DSC was for basal slices being around 0.92 on average with a low standard deviation. Both DSC and HD show a very compact performance of the obtained segmentation in global terms as well as the local description of RV shape. Nevertheless, the DSC decreases by around 0.1 from basal to apex. In the state-of-the-art, most methods report DSC over 0.9 [18,19,20] for basal slices. Additionally, adding apical slices decreases the DSC performance around 0.7. This indicates that increasing the segmentation performance for apical slices is a step forward. Most of the methods in the literature present problems with apex segmentation due to their appearance in MRI images, so creating models that do not rely fully on appearance for apical slices may improve the results. The segmentation error for apical slices is not considered a limiting factor for volume calculation. However, it can be critical for other types of applications and studies. Considering the inter-expert variability of 0.90 ± 0.10 [4], our methodology constitutes a potential tool to support automatic RV segmentation.

Table 2. RV Segmentation results; DSC ± standard deviation. Average HD in pixels.

	Measures	
	DSC (mean)	HD (mean)
Basal	0.92±0.05	4.19±1.54
All slices	0.87±0.12	4.20±1.41

Finally, in Table 3, the DSC obtained in our proposed method was compared with the best results obtained in the RVSC at MICCAI'12 [4]. These methods use different approaches, such as 4D watershed graph-cut segmentation [21], 2D multi-atlas registration [22], 3D multi-atlas registration [23] and 2D shape prior graph-cut segmentation [24]. Some of these methods need user inputs, i.e., are semi-automatic. For instance, O. Maier et al. [21] needs rough contouring of four to five 2D slices. The highest quantitative result of semi-automatic methods was the BIT-UPM, which reached a DSC of 0.80, while the best of the automatic methods (CMIC) reached 0.78. Compared to these state-of-art methodologies, our method works automatically by non-rigid registering atlases w.r.t an unknown MRI sequence (input) and, after a non-rectangular RoI detection, a probabilistic appearance model is applied to finally obtain an accurate segmentation achieving a DSC of 0.87.

Table 3. Comparison of Dice Score with best methods presented in the RVSC MICCAI 2012. All slices are considered.

RoI Approach	Basal	All slices
Proposed approach	Automatic	**0.87±0.12**
CMIC (M. Zuluaga et al.)	Automatic	0.78±0.23
SBIA (Y. Ou et al.)	Automatic	0.55±0.32
BIT-UPM (O. Maier et al.)	Semi-automatic	**0.80±0.19**
ICL (W. Bai et al.)	Semi-automatic	0.78±0.20
LITIS (D. Grosgeorge et al.)	Semi-automatic	0.76±0.20

4. DISCUSSION

This work introduced a method for RV segmentation from cardiac cine-MRI sequences by integrating spatio-temporal information into a compact DHT descriptor and a probabilistic model. RV spatial and motion deformation was herein modeled as a dense representation achieved by a DHT and a recursive probabilistic Bayesian model. An average template was firstly rigid registered to the new cardiac MRI sample as initial heart region estimation. The observations into the probabilistic model were defined as RV and background appearance representations. Complementary to the observations, a non-parametric shape characterization was defined as the result of a DHT, that allows to globally track the RV and locally update the appearance model. The DHT codes curvature and orientation at voxel level and follows non-linear changes on RV shape. The proposed approach was evaluated over the RVSC dataset, which includes a total of 16 patients. Also was evaluated in terms of the DSC for complete volumes and only basal RV structures, achieving rates of 0.87 and 0.92, respectively. These results outperformed the state-of-the-art methods, with the main advantage of the flexibility and independence of large training datasets. Additionally, this work was able to obtain RV segmentations along the cardiac cycle, without using any additional prior delineations.

Some of the RVSC works make use of different approaches, such as Atlas-based, shape prior-based, and prior-based methods (Table 3). In general, multi-atlas segmentation methods consist of two steps, specifically image registration (rigid or non-rigid) and label merging. ICL requires as input a few markers per volume to define a RoI and the registration process is carried out by a landmark-based image registration only in the RoI for the RV, while the CMIC has a pre-processing step to remove non-relevant structures before the registration. Also, SBIA performs straight image registration to the entire atlas w.r.t the target images, which directly affects its performance in terms of DSC. Nevertheless, these methods have some limitations which include accuracy performance dependence of the atlas/dataset quality, high computational cost due to registration between target and multiple atlases. Our approach overcomes these limitations by considering an RV shape prior as RoI and using a DH representation under a probabilistic appearance model. Finally, in [21], is reported a fully automatic joint segmentation of the left and right cardiac ventricles based on a graph cut framework by using a shape prior. The shape model is based on multi-atlas non-rigid registration and label merging. This methodology achieved a DSC average of 0.80 for end-diastole and end-systole. However, in the case of segmenting the right ventricle during the entire cardiac cycle, it is necessary to iterate the entire methodology without taking previous information into account. The proposed approach segmented the heart cycle over the entire scene without the need for additional information. This was possible due to prior information being taken into account for the current frame.

Our approach introduced a local characterization of the heart region over cine-MRI sequences. The characterization was achieved by computing a temporal Bayesian framework with a DHT that allows to localize the region of interest by using angle and curvature primitives over each pixel. The implemented characterization results fundamental to understand how the right heart ventricle shape changes over a cardiac cycle. This dense cardiac Hough characterization was applied in RV segmentation. In this scenario, the DHT is fundamental to follow non-parametric regions of interest and to code relevant information of the heart. Over a public dataset of 95 samples, the proposed strategy achieved an average score of 0.87 for all slices and 0.92 for basal slices only.

5. CONCLUSIONS

In this work was introduced a local characterization of the right ventricle over cine-MRI sequences. The characterization was achieved by computing a novel cardiac representation based on the dense Hough Transform and following a temporal Bayesian framework. This probabilistic method allows the adaptation of diverse multi-scale temporal changes during the cardiac cycle. The implemented characterization also allows to understand how right ventricle shape changes temporarily and achieves an accurate segmentation. The DHT results fundamental to follow and describe non-parametric regions of interest such as the RV. Future works will include the use of additional local primitives to model non-linear behavior of the heart in terms of its dynamics and shape. Also, an additional evaluation will be carried out with more rich datasets, for instance, the left ventricle will be included to evaluate the performance of the proposed approach. Additionally, a more exhaustive analysis will be carried out on the influence of the update factor (which was empirically set to a value of 0.1) on the final results.

6. ACKNOWLEDGEMENTS

7. REFERENCES

[1] World Health Organization. (2019). *World health statistics 2019: monitoring health for the SDGs, sustainable development goals*. World Health Organization.

[2] Labrador, A. M. A., Martínez, F., & Castro, E. R. (2013, November). A novel right ventricle segmentation approach from local spatio-temporal MRI information. In *Iberoamerican Congress on Pattern Recognition* (pp. 206-213). Springer, Berlin, Heidelberg.

[3] Bernard, O., Lalande, A., Zotti, C., Cervenansky, F., Yang, X., Heng, P. A., ... & Jodoin, P. M. (2018). Deep learning techniques for automatic MRI cardiac multi-structures segmentation and diagnosis: Is the problem solved? *IEEE transactions on medical imaging*, *37*(11), 2514-2525.

[4] Petitjean, C., Zuluaga, M. A., Bai, W., Dacher, J. N., Grosgeorge, D., Caudron, J., ... & Yuan, J. (2015). Right ventricle segmentation from cardiac MRI: a collation study. *Medical image analysis*, *19*(1), 187-202.

[5] Vanderpool, R. R., Pinsky, M. R., Naeije, R., Deible, C., Kosaraju, V., Bunner, C., ... & Simon, M. A. (2015). RV-pulmonary arterial coupling predicts outcome in patients referred for pulmonary hypertension. *Heart*, *101*(1), 37-43.

[6] Buchner, S., Eglseer, M., Debl, K., Hetzenecker, A., Luchner, A., Husser, O., ... & Arzt, M. (2015). Sleep disordered breathing and enlargement of the right heart after myocardial infarction. *European Respiratory Journal*, *45*(3), 680-690.

[7] Gilbert, K., Lam, H. I., Pontré, B., Cowan, B. R., Occleshaw, C. J., Liu, J. Y., & Young, A. A. (2017). An interactive tool for rapid biventricular analysis of congenital heart disease. *Clinical physiology and functional imaging*, *37*(4), 413-420.

[8] Petitjean, C., & Dacher, J. N. (2011). A review of segmentation methods in short axis cardiac MR images. *Medical image analysis*, *15*(2), 169-184.

[9] Winter, M. M., Bernink, F. J., Groenink, M., Bouma, B. J., van Dijk, A. P., Helbing, W. A., ... & Mulder, B. J. (2008). Evaluating the systemic right ventricle by CMR: the importance of consistent and reproducible delineation of the cavity. *Journal of Cardiovascular Magnetic Resonance*, *10*(1), 1-8.

[10] Tran, P. V. (2016). A fully convolutional neural network for cardiac segmentation in short-axis MRI. *arXiv preprint arXiv:1604.00494*.

[11] El-Rewaidy, H., Ibrahim, E. S., & Fahmy, A. S. (2016). Segmentation of the right ventricle in MRI images using a dual active shape model. *IET Image Processing*, *10*(10), 717-723.

[12] Sedai, S., Garnavi, R., Roy, P., & Liang, X. (2015, August). Multi-atlas label fusion using hybrid of discriminative and generative classifiers for segmentation of cardiac MR images. In *2015 37th Annual International Conference of the IEEE Engineering in Medicine and Biology Society (EMBC)* (pp. 2977-2980). IEEE.

[13] Xie, L., Sedai, S., Liang, X., Compas, C. B., Wang, H., Yushkevich, P. A., & Syeda-Mahmood, T. (2015, April). Multi-atlas label fusion with augmented atlases for fast and accurate segmentation of cardiac MR images. In *2015 IEEE 12th International Symposium on Biomedical Imaging (ISBI)* (pp. 376-379). IEEE.

[14] Zhen, X., Wang, Z., Islam, A., Bhaduri, M., Chan, I., & Li, S. (2016). Multi-scale deep networks and regression forests for direct bi-ventricular volume estimation. *Medical image analysis*, *30*, 120-129.

[15] Avendi, M. R., Kheradvar, A., & Jafarkhani, H. (2016). Fully automatic segmentation of heart chambers in cardiac MRI using deep learning. *Journal of Cardiovascular Magnetic Resonance*, *18*(1), 1-3.

[16] Manzanera, A. (2012). Dense Hough transforms on gray level images using multi-scale derivatives. In *SIXIEME WORKSHOP AMINA 2012" Applications Médicales de l'Informatique: Nouvelles Approches"*.

[17] Duffner, S., & Garcia, C. (2013). Pixeltrack: a fast adaptive algorithm for tracking non-rigid objects. In *Proceedings of the IEEE international conference on computer vision* (pp. 2480-2487).

[18] Luo, G., An, R., Wang, K., Dong, S., & Zhang, H. (2016, September). A deep learning network for right ventricle segmentation in short-axis MRI. In *2016 Computing in Cardiology Conference (CinC)* (pp. 485-488). IEEE.

[19] El-Rewaidy, H., Ibrahim, E. S., & Fahmy, A. S. (2016). Segmentation of the right ventricle in MRI images using a dual active shape model. *IET Image Processing*, *10*(10), 717-723.

[20] El-Rewaidy, H., & Fahmy, A. S. (2015, April). Segmentation of the Right Ventricle in MR images using dual active shape model in the Bookstein coordinates. In *2015 IEEE 12th International Symposium on Biomedical Imaging (ISBI)* (pp. 1320-1323). IEEE.

[21] Maier, O. M., Jiménez, D., Santos, A., & Ledesma-Carbayo, M. J. (2012). Segmentation of RV in 4D cardiac MR volumes using region-merging graph cuts. In *2012 Computing in Cardiology* (pp. 697-700). IEEE.

[22] Zuluaga, M. A., Cardoso, M. J., Modat, M., & Ourselin, S. (2013). Multi-atlas propagation whole heart segmentation from MRI and CTA using a local normalised correlation coefficient criterion. In *International Conference on Functional Imaging and Modeling of the Heart* (pp. 174-181). Springer, Berlin, Heidelberg.

[23] Bai, W., Shi, W., Wang, H., Peters, N. S., & Rueckert, D. (2012). Multiatlas based segmentation with local label fusion for right ventricle MR images. *image*, *6*, 9.

[24] Grosgeorge, D., Petitjean, C., Dacher, J. N., & Ruan, S. (2013). Graph cut segmentation with a statistical shape model in cardiac MRI. *Computer Vision and Image Understanding*, *117*(9), 1027-1035.